Geophys. J. Int. (1994) **118,** 317–324

Non-axisymmetric guided waves in a composite cylinder with transversely isotropic core

N. Rattanawangcharoen,[1] Subhendu K. Datta[2,*] and Arvind H. Shah[3]

[1] *Department of Civil Engineering, Faculty of Engineering, Chiang Mai University, Chiang Mai, 50002, Thailand*
[2] ER-15, *Division of Engineering and Geosciences, Office of Basic Energy Sciences, US Department of Energy, Washington,* DC 20595, *USA*
[3] *Department of Civil and Geological Engineering, University of Manitoba, Winnipeg,* R3T 2N2, *Canada*

Accepted 1994 January 21. Received 1994 January 13

SUMMARY

Ultrasonic guided waves in a composite cylinder have been studied by using a Rayleigh–Ritz-type finite-element representation. Although the method can be applied to general anisotropic cylinders, the analysis has been confined here to the case of a narrow transversely isotropic solid cylindrical core surrounded by a thick coaxial isotropic cylinder. Numerical results are presented for the dispersion of the first two modes when the circumferential wavenumber $n = 1$ and 3. It is found that, for the particular case of a graphite core in a magnesium cylinder, the two modal branches approach very closely (pinch) at the Rayleigh wave speed of magnesium. In the presence of a soft interface material, the pinch frequency is found to shift downwards. The effect of this interface material on the dispersion is also discussed.

Key words: composite cylinder, guided wave, interface dispersion, transversely isotropic.

1 INTRODUCTION

Fibre-reinforced composite materials are widely used in aerospace and mechanical engineering. Clad rods or wires have been investigated for use as acoustic delay lines and fibre acoustic waveguides. In recent years, there have been several investigations dealing with guided waves in isotropic clad rods (fibres). A survey of the early literature was given by Thurston (1978). More recently, fibre acoustic waveguides have been investigated by Safaai-Jazi, Jen & Farnell (1986) under the assumption of weak guidance. The equation governing the dispersion of guided waves in a cladded cylinder is complicated, even when both materials are isotropic. They are much more complicated if the materials are anisotropic. Previously, several studies have dealt with acoustic propagation in uncladded transversely isotropic rods. For references the reader is referred to Xu & Datta (1991) and Dai *et al.* (1992a,b). Because of the algebraic complexity of anisotropic wave propagation, Xu & Datta (1991) used a hybrid method to study acoustic waves in a composite waveguide having a thin hexagonal core surrounded by a thick isotropic coaxial cylinder. Their study was limited to the case of axisymmetry. Dai *et al.* (1992a,b) presented an analytical solution for the case of non-axisymmetric wave propagation in single-crystal cladded fibres having a hexagonal core and a hexagonal cladding. They presented numerical results, however, only for the weak guidance case and when the cladding is infinitely thick.

In this paper we consider non-axisymmetric waves in a cladded rod having a transversely isotropic core and an isotropic cladding. The method of analysis is based upon a Rayleigh–Ritz-type finite-element representation. Discretization in the radial direction is used to model the radial variation of the constitutive properties. The advantage of the method is that arbitrary anisotropy and many layers can be considered. This allows us to examine the effect of a soft interface material on the changes in the dispersion characteristics. The objective here is to assess the feasibility of an ultrasonic technique to characterize interface material properties.

2 THEORY

Consider a layered cylinder, as shown in Fig. 1. Fig. 1(a) shows the coordinate system (r, θ, z). The materials are assumed to be linearly elastic, anisotropic in the core and isotropic in the interface and matrix regions. The layer parameters are r_{l-1} (inner radius), r_l (outer radius), ρ^l (density) and C_{ij}^l (elastic constants in the contracted notation) where $i, j = 1, \ldots, 6$. The superscript $l = \mathrm{I}, \mathrm{II}, \mathrm{III}$

* Permanent address: Department of Mechanical Engineering University of Colorado, Boulder, CO 80309-0427, USA.

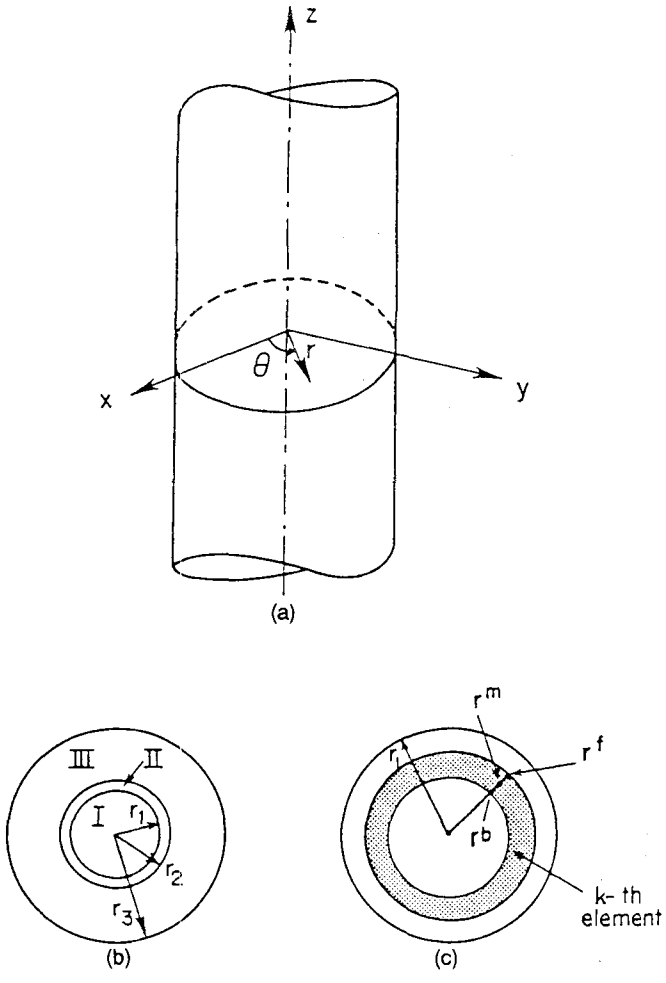

Figure 1. Geometry of the problem.

and subscript $l = 1, 2, 3$, are associated with the core, interface layer and outer matrix layer, respectively.

As discussed in Xu & Datta (1991), the wave equations that govern the displacement in the layers can be solved for wave propagation in the axial (z-) direction in the form

$$u_r = \sum_{n=0}^{\infty} U_r^n(r, z, t) \cos n\theta,$$
$$u_\theta = \sum_{n=0}^{\infty} U_\theta^n(r, z, t) \sin n\theta, \qquad (1)$$
$$u_z = \sum_{n=0}^{\infty} U_z^n(r, z, t) \cos n\theta,$$

where u_r, u_θ, u_z are the components of displacement in the r-, θ-, z-directions, respectively. The equations governing U_r^n, U_θ^n, U_z^n are coupled in general. For the isotropic case, they can be obtained from the potentials which are governed by equations that are uncoupled. For a generally anisotropic material, such a simplification can not be accomplished. If the material is transversely isotropic, having the z-axis as the axis of symmetry, one can also represent U_r^n, U_θ^n, U_z^n in terms of potentials that satisfy uncoupled equations. However, in the latter case, the solutions are rather complicated. For this reason and for reasons of general applicability, we have adopted a finite-element technique to solve the free guided wave problem for the composite cylinder.

2.1 Finite-element representation

In the finite-element representation, we divide the composite cylinder into concentric shells. Within each shell the displacement variation in the radial direction is approximated by a quadratic polynomial with coefficients that are the generalized displacements. Thus, for circumferential wavenumber n, we assume that

$$\{\mathbf{U}\} = [\mathbf{N}]\{\mathbf{q}\}, \qquad (2)$$

where the components of $\{\mathbf{U}\}$ are U_r^n, U_θ^n, U_z^n, as defined in eqs (1). Furthermore,

$$\{\mathbf{q}\} = \langle u_r^b, u_\theta^b, u_z^b, u_r^m, u_\theta^m, u_z^m, u_r^f, u_\theta^f, u_z^f \rangle^{\mathrm{T}},$$
$$[\mathbf{N}] = \begin{bmatrix} n_1 & 0 & 0 & n_2 & 0 & 0 & n_3 & 0 & 0 \\ 0 & n_1 & 0 & 0 & n_2 & 0 & 0 & n_3 & 0 \\ 0 & 0 & n_1 & 0 & 0 & n_2 & 0 & 0 & n_3 \end{bmatrix}, \qquad (3)$$

where the superscripts b, m, f represent the values at the nodes of the kth element which are at r_{k-1}, $\frac{1}{2}(r_k + r_{k-1})$, r_k, $(r_{k-1} < r < r_k)$. The interpolation polynomials n_i, $i = 1, 2, 3$, are given by

$$n_1(\zeta) = 1 - 3\zeta + 2\zeta^2, \qquad n_2(\zeta) = 4\zeta - 4\zeta^2,$$
$$n_3(\zeta) = -\zeta + 2\zeta^2, \qquad \zeta = (r - r_{k-1})/(r_k - r_{k-1}). \qquad (4)$$

In eq. (2) we have dropped the superscript n for convenience. Substituting eq. (2) into the strain–displacement relations, it is found that (see Xu & Datta 1991)

$$\{\boldsymbol{\epsilon}\} = [\mathbf{b}](\partial/\partial z)\{\mathbf{q}\} + [\mathbf{a}]\{\mathbf{q}\}, \qquad (5)$$

where $[\mathbf{a}]$ and $[\mathbf{b}]$ are real matrices, defined in the Appendix, and

$$\{\boldsymbol{\epsilon}\} = \langle \epsilon_{rr}, \epsilon_{\theta\theta}, \epsilon_{zz}, \gamma_{\theta z}, \gamma_{zr}, \gamma_{r\theta} \rangle^{\mathrm{T}}. \qquad (6)$$

The equation governing the nodal displacement is obtained by using Hamilton's principle. For this purpose, consider the Lagrangian for each element:

$$L = \frac{1}{2} \int_t \int_z \int_r \int_\theta \times \left(\rho \frac{\partial}{\partial t} \{\mathbf{U}^*\}^{\mathrm{T}} \frac{\partial}{\partial t} \{\mathbf{U}\} - \{\boldsymbol{\epsilon}^*\}^{\mathrm{T}} [\mathbf{C}] \{\boldsymbol{\epsilon}\} \right) r \, dr \, d\theta \, dz \, dt, \qquad (7)$$

where ρ is the mass density and $[\mathbf{C}]$ the 6×6 symmetric elastic stiffness matrix. The asterisk denotes a complex conjugate.

Substituting eqs (2) and (5) into eq. (7) and integrating over the circumferential and radial coordinates, we obtain

$$\pi^{-1} L = \int_t \int_z (\{\dot{\mathbf{q}}^*\}^{\mathrm{T}} [\mathbf{m}] \{\dot{\mathbf{q}}\} - \{\mathbf{q}'^*\}^{\mathrm{T}} [k_1] \{\mathbf{q}'\} - \{\mathbf{q}'^*\}^{\mathrm{T}} [k_2] \{\mathbf{q}\} - \{\mathbf{q}^*\}^{\mathrm{T}} [k_2]^{\mathrm{T}} \{\mathbf{q}'\} - \{\mathbf{q}^*\}^{\mathrm{T}} [k_3] \{\mathbf{q}\}) \, dz \, dt, \qquad (8)$$

where prime and dot denote differentiation with respect to z and t, respectively. The mass matrix $[\mathbf{m}]$ and the

stiffness-related matrices $[\mathbf{k}_1]$, $[\mathbf{k}_2]$, $[\mathbf{k}_3]$ are defined as

$$[\mathbf{m}] = \int_r \rho[\mathbf{N}]^{\mathrm{T}}[\mathbf{N}]r\,dr, \qquad [\mathbf{k}_1] = \int_r [\mathbf{b}]^{\mathrm{T}}[\mathbf{C}][\mathbf{b}]r\,dr,$$
$$[\mathbf{k}_2] = \int_r [\mathbf{b}]^{\mathrm{T}}[\mathbf{C}][\mathbf{a}]r\,dr, \qquad [\mathbf{k}_3] = \int_r [\mathbf{a}]^{\mathrm{T}}[\mathbf{C}][\mathbf{a}]r\,dr. \tag{9}$$

The integrations specified in eqs (9) can be computed exactly if the density ρ and stiffness $[\mathbf{C}]$ are constants within each shell. Otherwise, they can be obtained by numerical integration. It is observed that $[\mathbf{k}_1]$ and $[\mathbf{k}_3]$ are symmetric, whereas $[\mathbf{k}_2]$ is not.

Assembling the Lagrangians for all the elements, we can find the total Lagrangian for the composite cylinder. Setting the first variation of the Lagrangian to zero gives the second-order partial differential equations

$$-[\mathbf{K}_1]\frac{\partial^2}{\partial z^2}\{\tilde{\mathbf{Q}}\} + ([\mathbf{K}_2]^{\mathrm{T}} - [\mathbf{K}_2])\frac{\partial}{\partial z}\{\tilde{\mathbf{Q}}\}$$
$$+ [\mathbf{K}_3]\{\tilde{\mathbf{Q}}\} + [\mathbf{M}]\frac{\partial^2}{\partial t^2}\{\tilde{\mathbf{Q}}\} = 0. \tag{10}$$

In the above, $\{\tilde{\mathbf{Q}}\}$ is the global nodal displacement vector, $[\mathbf{M}]$ is the global mass matrix and $[\mathbf{K}_1]$, $[\mathbf{K}_2]$, $[\mathbf{K}_3]$ are global stiffness-related matrices. It has been assumed that there are no external forces acting on the cylinder.

If we now assume the t and z dependence of the displacement components in the form $\tilde{Q} = \tilde{Q}_0 \exp[i(\xi z - \omega t)]$, then

$$\partial/\partial z = i\xi, \qquad \partial/\partial t = -i\omega = -ic\xi, \tag{11}$$

and we obtain from eq. (10)

$$(\xi^2[\mathbf{K}_1] + i\xi([\mathbf{K}_2]^{\mathrm{T}} - [\mathbf{K}_2]) + [\mathbf{K}_3] - \omega^2[\mathbf{M}])\{\tilde{\mathbf{Q}}_0\} = 0. \tag{12}$$

For a non-trivial solution, the determinant of the coefficient matrix of $\{\tilde{\mathbf{Q}}_0\}$ must be zero. This leads to the eigenvalue problem for the determination of the wavenumber ξ for a given frequency ω.

In Xu & Datta (1991), a somewhat different hybrid technique was used to study the guided waves in the composite cylinder. In this alternative method, the finite-element formulation was used only for the core. The resulting equations were coupled to the analytical solution for the isotropic interface and outer matrix materials. This has the advantage that the outer radius of the matrix region can extend to infinity. Results of the two methods were shown to agree quite well for the composite cylinder having a finite outer radius. Here, we have used the finite-element representation to study the non-axisymmetric waves.

3 NUMERICAL RESULTS AND DISCUSSION

The present study is focused on the dispersion of graphite fibre in a magnesium matrix. The material properties of the fibre (core), interface and matrix regions are given in Table 1. The radius of the core is taken to be 1 mm and the outer radius of the matrix (magnesium) cylinder is fixed at 11 mm. The thickness of the interface region between the core and the matrix is varied: 0, 0.1 and 0.2 mm.

For the numerical computations, the finite-element Rayleigh–Ritz procedure was used. For this purpose, the core was divided into five concentric cylinders with radius increments of 0.20 mm. The interface region was divided into two or four concentric cylinders of equal thickness (0.05 mm). The magnesium annular region was divided into 60, 58 or 56 concentric annuli, respectively, for the three interface thicknesses (0, 0.1 and 0.2 mm). Thus, for the maximum frequency considered (10 MHz), the wavelength of the shear wave in magnesium is about four times the distance between two adjacent nodes. The results were verified by comparison with those reported in Xu & Datta (1991) for $n = 0$.

Table 1. Material properties: densities in gm cm^{-3}, elastic constants in GPa.

Property	Graphite	Interphase	Magnesium
ρ	2.269	1.738	1.738
C_{11}	20.02	10.94	109.4
C_{33}	234.77	10.94	109.4
C_{12}	9.98	5.70	57.0
C_{13}	6.45	5.70	57.0
C_{55}	24.00	2.62	26.2
C_{66}	5.02	2.62	26.2

Equation (12) provides a set of roots for ξ for a given frequency ω. Not all of these roots are real. The real roots correspond to the propagating modes. For $n \leq 1$, there is one propagating mode for all ω. This is the lowest mode and is called the longitudinal mode when $n = 0$ and the flexural mode for $n = 1$. All higher modes have cut-off frequencies below which they become evanescent (ξ complex) or non-propagating (ξ imaginary). In this paper we have focused our attention on the two lowest modes for $n = 1$ and 3. Our interest is to delineate the characteristics of these two modes as they depend on the anisotropic core and isotropic interface properties.

The material properties of graphite and magnesium are such that the longitudinal (P) wave speed of the former in the z-direction (V_{33}^{f}) is higher than that of the latter, whereas the axial-shear (SH) wave speed of graphite (V_{55}^{f}) is lower than that in magnesium. Also, graphite is strongly anisotropic (V_{33}^{f} is more than three times larger than V_{55}^{f}). For reference, these speeds are noted as $V_{55}^{\mathrm{f}} = 3.25\ \mathrm{mm}\,\mu\mathrm{s}^{-1}$ ($= 3250\ \mathrm{m\,s}^{-1}$), $V_{33}^{\mathrm{f}} = 10.17\ \mathrm{mm}\,\mu\mathrm{s}^{-1}$, $V_{33}^{\mathrm{m}} = 6.94\ \mathrm{mm}\,\mu\mathrm{s}^{-1}$, $V_{55}^{\mathrm{m}} = 3.88\ \mathrm{mm}\,\mu\mathrm{s}^{-1}$. Fig. 2 shows the dispersion curves for the first two branches of the flexural ($n = 1$) mode. This figure shows speed in $\mathrm{mm}\,\mu\mathrm{s}^{-1}$ (vertical axis) *versus* frequency in MHz (horizontal axis). It is seen that the speed of the lowest branch increases rapidly with frequency and reaches a plateau at the Rayleigh wave speed of magnesium, $V_r^{\mathrm{m}} = 3.63\ \mathrm{mm}\,\mu\mathrm{s}^{-1}$. The speed of the next higher branch, which has a cut-off frequency of 0.11 MHz, decreases rapidly and approaches gradually a short plateau at the shear-wave speed of magnesium, $V_{55}^{\mathrm{m}} = 3.88\ \mathrm{mm}\,\mu\mathrm{s}^{-1}$. Then it drops gradually to V_r^{m} when this branch almost touches the flexural branch at about 1.39 MHz. The speed of the lowest (flexural) branch then drops gradually to the axial-shear-wave speed of graphite, $3.25\ \mathrm{mm}\,\mu\mathrm{s}^{-1}$. On the other hand, the speed of the second mode reaches a plateau after the pinch frequency at V_r^{m} and then, at about 2.7 MHz, it too drops gradually to V_{55}^{f}.

To understand the mode interchange that occurs at the pinch frequency of the first two modes, Fig. 3 shows the

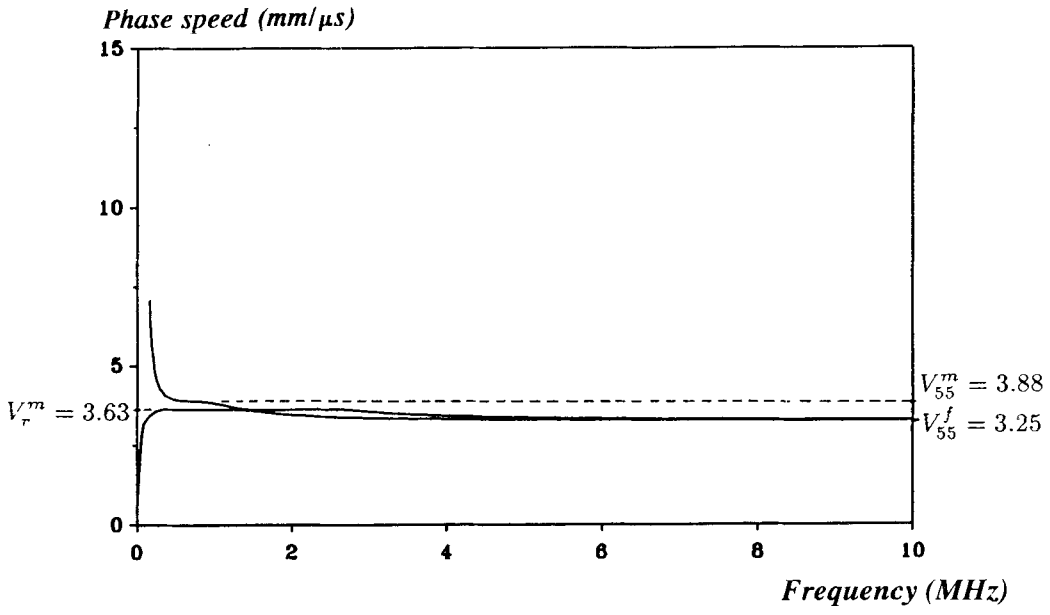

Figure 2. Dispersion curves for a graphite fibre in a magnesium rod. Circumferential wavenumber $n = 1$.

mode shapes associated with these two branches. Figs 3(b) and (d) show the shapes associated with the first branch before and after the pinch frequency and Figs 3(c) and (e) show those for the second branch. It is seen that below this frequency the motion associated with the first branch is confined to the outer surface of the magnesium cylinder, whereas above it the motion is in the graphite core. The second branch shows just the opposite behaviour.

Figures 4 and 5 show the effect of a soft interface layer of thickness 0.1 and 0.2 mm, respectively. Now it is found that the pinch frequency is about 0.9 MHz for the 0.1 mm interface and 0.7 MHz for the 0.2 mm interface. Also, it is

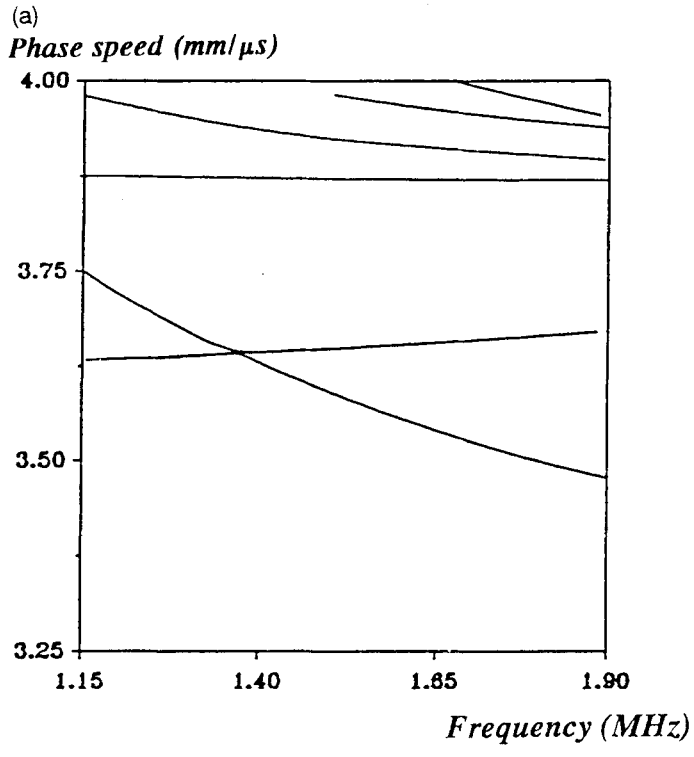

Figure 3. (a) Close-up view of the first two branches of the curves shown in Fig. 2 near the pinch frequency; (b) and (d) mode shapes associated with the first branch before and after this frequency; (c) and (e) mode shapes associated with the second branch. —— radial component, - - - axial component, ——— transverse component.

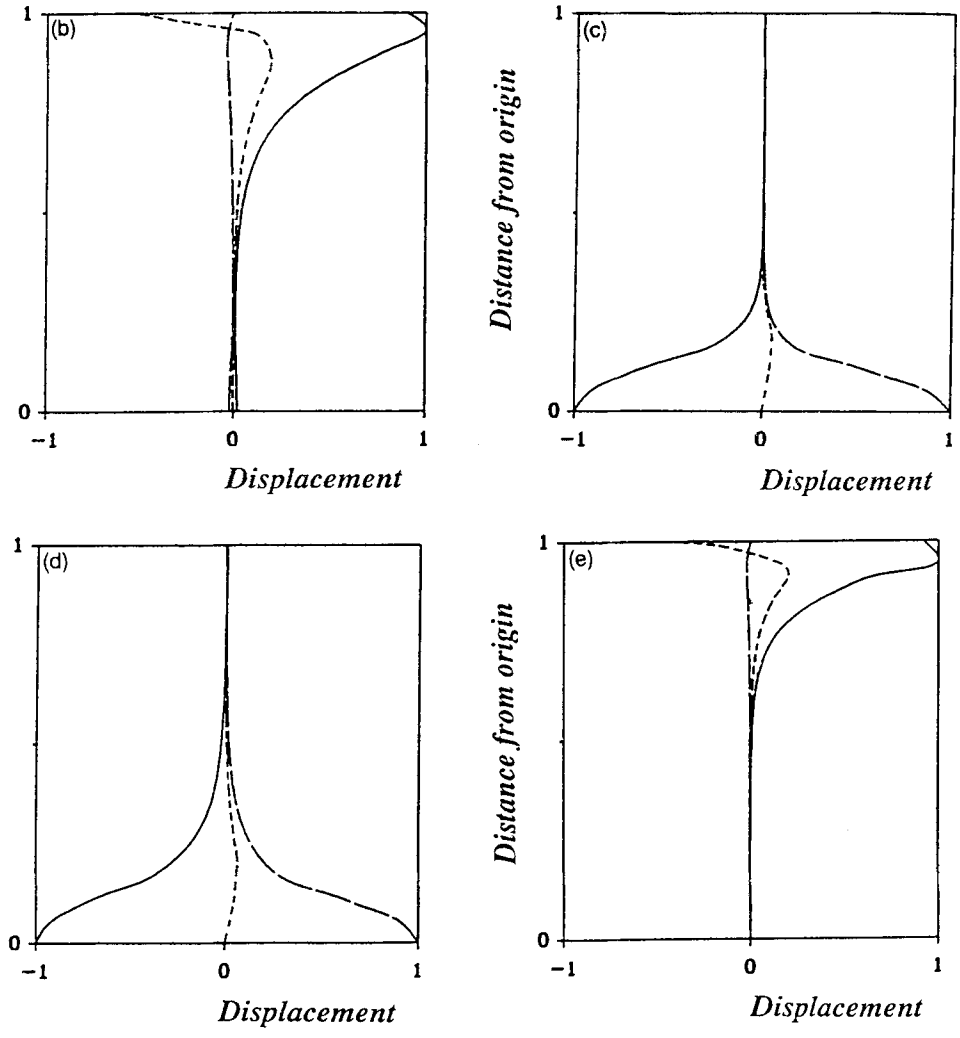

Figure 3. (*Continued*)

noted that the speed of the second branch starts dropping at about 2.0 and 1.6 MHz in the two cases, respectively. Thus, the presence of the interface decreases these transition frequencies measurably. The other distinct feature is that the soft interface material causes the speeds of these branches to drop gradually below V_{55}^{f}. Fig. 5 shows that they asymptotically approach the shear-wave speed of the interface material, $V_s^i = 1.23\,\text{mm}\,\mu\text{s}^{-1}$.

Figures 6–8 show the first two branches for $n = 3$. They show very similar behaviour as for $n = 1$. In this case there is a cut-off frequency below which there are no propagating modes. Above this frequency, the speed of the first branch drops rapidly and plateaus to V_r^m first (Fig. 6). On the other hand, the speed of the second branch drops first to V_{55}^m and then this branch pinches the first at speed V_r^m at about 3.3 MHz. Following this, the two branches behave like the $n = 1$ modes. Figs 7 and 8 show the effect of the interface layer. Again, the transition frequencies are lower in the presence of this layer.

The pinching and transition behaviour is characteristic of a bilayer cylinder when the material properties are significantly different. The presence of the strongly anisotropic core makes the transition rather sharp. These features could be exploited to determine the material properties of the constituents as well as those of an interface layer.

4 CONCLUSIONS

Guided waves in cladded fibres have been studied in this paper. The fibre is assumed to have transverse isotropy with the axis of symmetry aligned with its axis. A Rayleigh–Ritz-type finite-element procedure had been used to analyse the dispersive behaviour of non-axisymmetric waves. Numerical results are presented for the case of a graphite fibre surrounded by a coaxial isotropic magnesium cylinder. Attention has been focused on the first two branches for the circumferential wavenumber, $n = 1$ and 3. It has been shown that there exist certain transition frequencies at which sharp changes occur. These frequencies are found to depend on the properties of the interface layer. For a soft interface, these frequencies shift downwards. The distinctive features of the guided waves could be used for ultrasonic characterization of the constituent and interface properties.

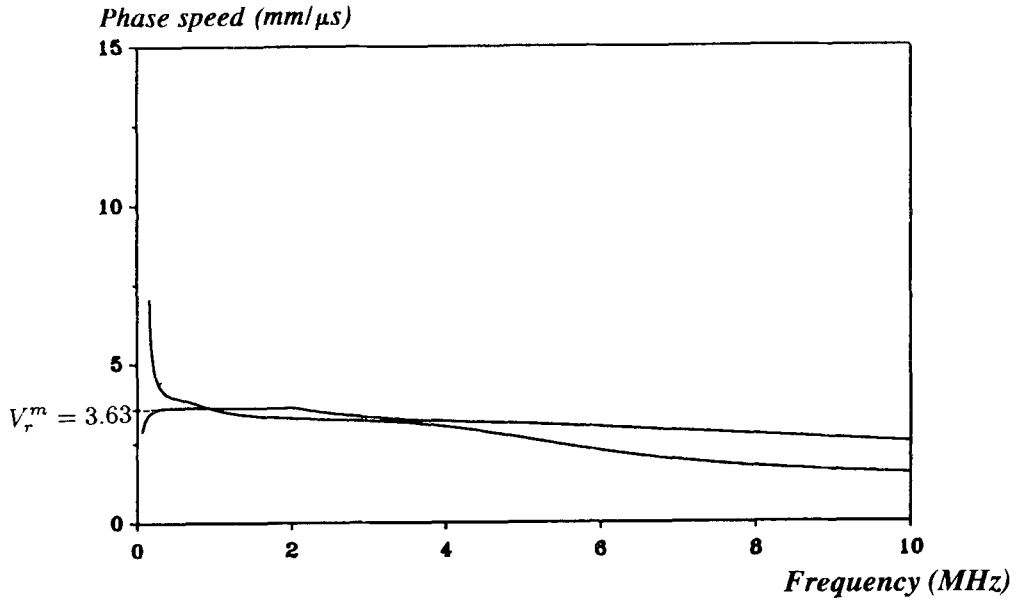

Figure 4. Dispersion curves for $n = 1$ when there is an interface layer between the fibre and the cladding. The interface layer thickness is 0.1 mm.

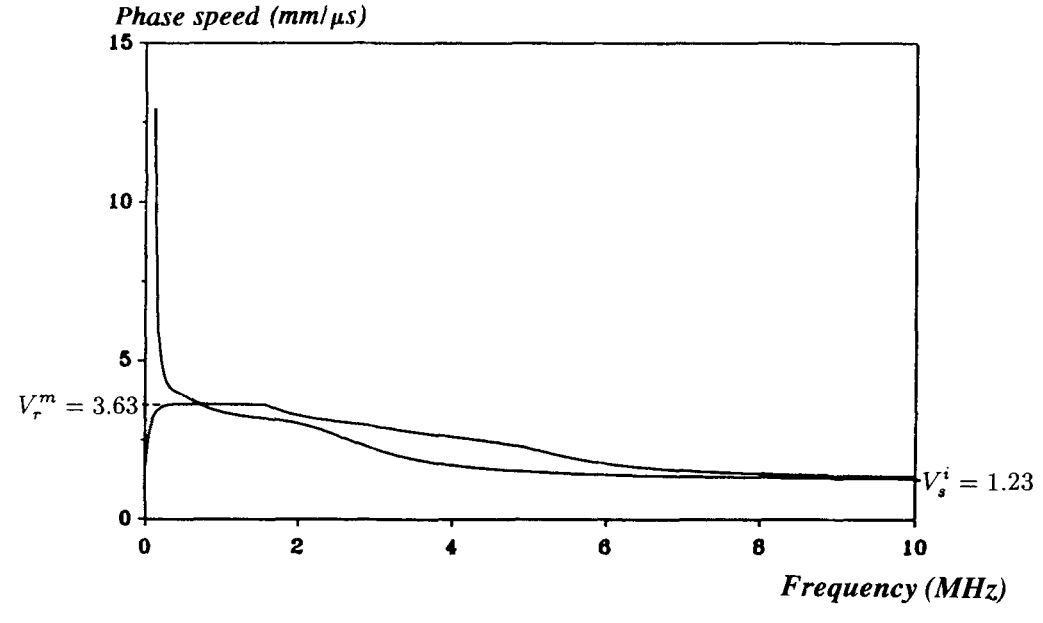

Figure 5. Same as Fig. 4 when the interface layer thickness is 0.2 mm.

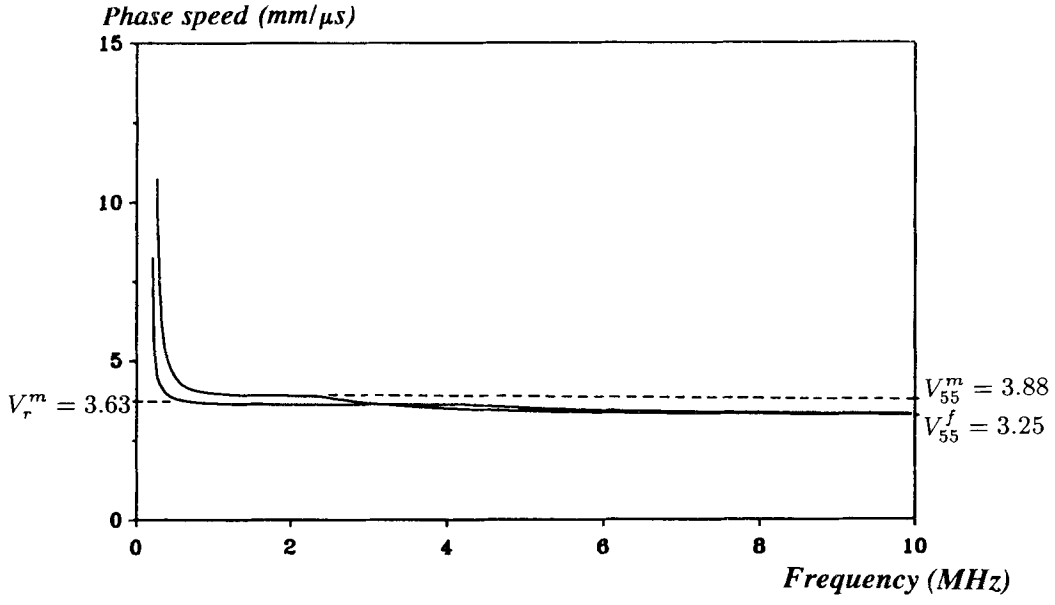

Figure 6. Same as Fig. 2 for $n = 3$.

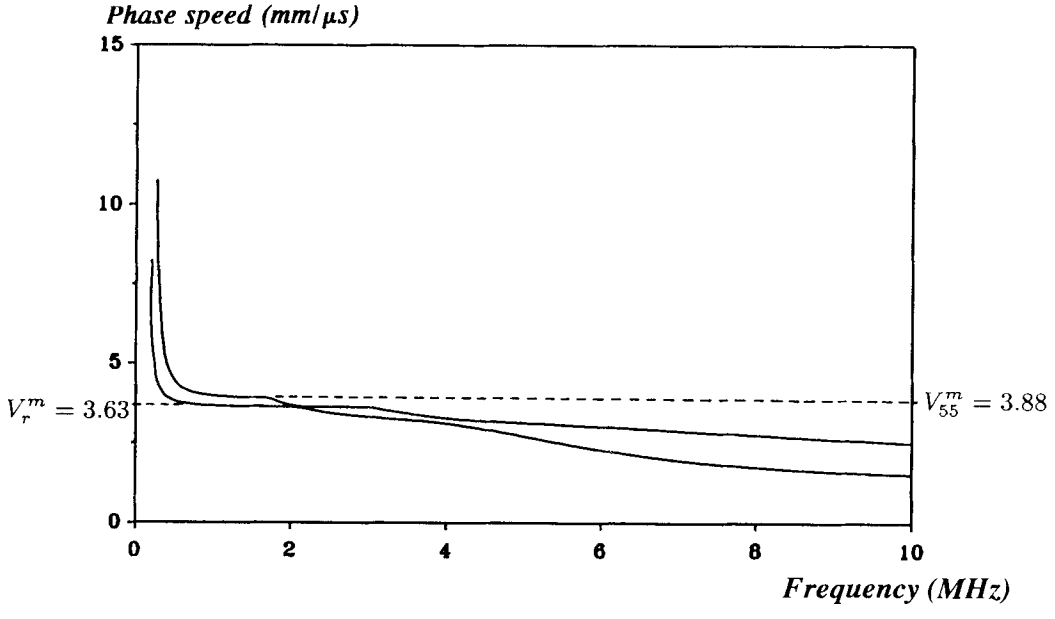

Figure 7. Dispersion curves for $n = 3$ when there is an interface layer between the fibre and the cladding. The interface layer thickness is 0.1 mm.

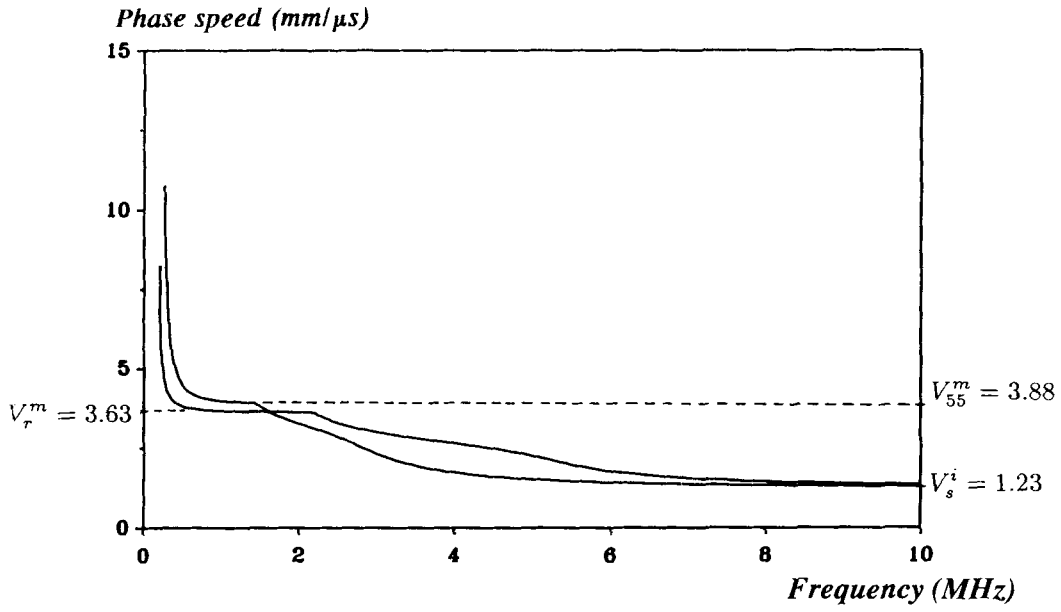

Figure 8. Same as Fig. 7 when the interface layer thickness is 0.2 mm.

ACKNOWLEDGMENT

The work reported here was supported in part by a grant (No. 0GP-0007988) from the Natural Science and Engineering Research Council.

REFERENCES

Dai, J.D., Winkel, V., Oliviera, J.E.B. & Jen, C.K., 1992a. Analysis of weakly guided cladded acoustic fibers of hexagonal crystal symmetry, *IEEE Trans. Ultrason. Ferroelectr. Freq. Contrib.*, **39**, 722–729.

Dai, J.D., Winkel, V., Oliviera, J.E.B. & Jen, C.K., 1992b. Analysis of cladded acoustic fibres of hexagonal symmetry, *IEEE Trans. Ultrason. Ferroelectr. Freq. Contrib.*, **39**, 730–736.

Safaai-Jazi, A., Jen, C.K. & Farnell, G.W., 1986. Analysis of weakly guiding fiber acoustic waveguide, *IEEE Trans. Ultrason. Ferroelectr. Freq. Contrib.*, **33**, 59–73.

Thurston, R.N., 1978. Elastic waves in rods and clad rods, *J. acoust. Soc. Am.*, **64**, 1–37.

Xu, P.C. & Datta, S.K., 1991. Characterization of fiber-matrix interface by guided waves: axisymmetric case, *J. acoust. Soc. Am.*, **89**, 2573–2583.

APPENDIX: DEFINITION OF MATRICES [a] AND [b]

The matrices [**a**] and [**b**] in eq. (5) are defined as

$$[\mathbf{a}] = \begin{bmatrix} \frac{dn_1}{dr} & 0 & 0 & \frac{dn_2}{dr} & 0 & 0 & \frac{dn_3}{dr} & 0 & 0 \\ \frac{n_1}{r} & \frac{nn_1}{r} & 0 & \frac{n_2}{r} & \frac{nn_2}{r} & 0 & \frac{n_3}{r} & \frac{nn_3}{r} & 0 \\ 0 & 0 & 0 & 0 & 0 & 0 & 0 & 0 & 0 \\ 0 & 0 & -\frac{nn_1}{r} & 0 & 0 & -\frac{nn_2}{r} & 0 & 0 & -\frac{nn_3}{r} \\ 0 & 0 & \frac{dn_1}{dr} & 0 & 0 & \frac{dn_2}{dr} & 0 & 0 & \frac{dn_3}{dr} \\ -\frac{nn_1}{r} & \frac{dn_1}{dr} - \frac{n_1}{r} & 0 & -\frac{nn_2}{r} & \frac{dn_2}{dr} - \frac{n_2}{r} & 0 & -\frac{nn_3}{r} & \frac{dn_3}{dr} - \frac{n_3}{r} & 0 \end{bmatrix},$$

$$[\mathbf{b}] = \begin{bmatrix} 0 & 0 & 0 & 0 & 0 & 0 & 0 & 0 & 0 \\ 0 & 0 & 0 & 0 & 0 & 0 & 0 & 0 & 0 \\ 0 & 0 & n_1 & 0 & 0 & n_2 & 0 & 0 & n_3 \\ 0 & n_1 & 0 & 0 & n_2 & 0 & 0 & n_3 & 0 \\ n_1 & 0 & 0 & n_2 & 0 & 0 & n_3 & 0 & 0 \\ 0 & 0 & 0 & 0 & 0 & 0 & 0 & 0 & 0 \end{bmatrix}.$$